CXCR4 blockade alleviates pulmonary and cardiac outcomes in young COPD

Isabelle Dupin[1,2], Pauline Henrot[1,2,3], Elise Maurat[1,2], Reshed Abohalaka[1,2], Sébastien Chaigne[1,2,3], Dounia El Hamrani[1,2], Edmée Eyraud[1,2], Renaud Prevel[1,2,3], Pauline Esteves[1,2], Maryline Campagnac[1,2], Marielle Dubreuil[1,2], Guillaume Cardouat[1,2], Clément Bouchet[1,2], Olga Ousova[1,2], Jean-William Dupuy[1,2], Thomas Trian[1,2], Matthieu Thumerel[1,2,3], Hugues Bégueret[1,2,3], Pierre-Olivier Girodet[1,2,3], Roger Marthan[1,2,3], Maeva Zysman[1,2,3], Véronique Freund-Michel[1,2], Patrick Berger[1,2,3]

[1] Univ. Bordeaux, Centre de Recherche Cardio-thoracique de Bordeaux, INSERM U1045, IHU Liryc, CIC 1401, Proteomics Facility, F-33600 Pessac, France

[2] INSERM, Centre de Recherche Cardio-thoracique de Bordeaux, U1045, CIC 1401, F-33600 Pessac, France

[3] CHU Bordeaux, Service d'exploration fonctionnelle respiratoire, Service de réanimation, Service de pneumologie, Service de chirurgie thoracique, Service de cardiologie-électrophysiologie et stimulation cardiaque, Service d'anatomopathologie, CIC-P 1401, F-33600 Pessac, France

Corresponding author: Prof. Isabelle Dupin

Centre de Recherche Cardio-thoracique de Bordeaux, INSERM U1045

PTIB. Hôpital Xavier Arnozan. Avenue du Haut Lévêque. 33600 Pessac

e-mail : isabelle.dupin@u-bordeaux.fr

“Take home” message:

The CXCL12/CXCR4 axis plays an important role in the pathogenesis of young COPD. Inhibition of this axis improves lung function and cardiac tissue remodelling, supporting the future use of CXCR4 inhibitors to slow down the progression of the disease.

Authors’ contribution:

- conception and design (ID, PB)
- data acquisition (ID, PH, EM, RA, SC, DEH, EE, PE, MC, MD, GC, CB, OO, JWD, TT, VFM)
- data analysis (ID, PH, EM, RA, SC, DEH, RP, MD, GC, CB, JWD, VFM, PB)
- data interpretation (ID, PH, EM, RA, SC, DEH, EE, RP, PE, MD, GC, CB, TT, RM, MZ, VFM, PB)
- resources (PH, MC, MD, MT, HB, POG, MZ, PB)
- drafting the manuscript (ID, PH, PB)
- revision and final approval of the version to be published, agreement to be accountable for all aspects of the work in ensuring that questions related to the accuracy or integrity of any part of the work are appropriately investigated and resolved (All)

Conflict-of-interest statement:

ID has 2 patents delivered (i) (EP N°3050574 *i.e.*, Use of plerixafor for treating and/or preventing acute exacerbations of chronic obstructive pulmonary disease); (ii) (EP N°20173595.8 *i.e.*, New compositions and methods of treating COVID-19 Disease). ID report a grant from the "Fondation Bordeaux Université," with funding from "Assistance Ventilatoire à Domicile" (AVAD) and "Fédération Girondine de Lutte contre les Maladies Respiratoires" (FGLMR).

PH reports non-financial support from AVAD and Chiesi, outside the submitted work and a grant from the "Fondation Bordeaux Université," with funding from AVAD and FGLMR.

POG reports grants, personal fees and non-financial support from AstraZeneca, personal fees and non-financial support from Chiesi, personal fees and non-financial support from GlaxoSmithKline, personal fees and non-financial support from Novartis, personal fees and non-financial support from Sanofi, outside the submitted work. POG has 2 patents delivered (i) (EP N°3050574 *i.e.*, Use of plerixafor for treating and/or preventing acute exacerbations of chronic obstructive pulmonary disease); (ii) (EP N°20173595.8 *i.e.*, New compositions and methods of treating COVID-19 Disease).

MZ reports personal fees from AstraZeneca, Boehringer Ingelheim, CSL Behring, Novartis, Chiesi, GlaxoSmithKline and non-financial support Lilly outside the submitted work and a grant from the "Fondation Bordeaux Université," with funding from AVAD and FGLMR.

PB is the medical coordinator of the French national cohort (*i.e.*, COBRA), which received grants from AstraZeneca, GlaxoSmithKine, and Chiesi. Moreover, PB reports grants and personal fees from Novartis, personal fees and non-financial support from Chiesi, grants, personal fees and non-financial support from Boehringer Ingelheim, grants, personal fees and non-financial support from AstraZeneca, personal fees and non-financial support from GSK, personal fees and non-financial support from Sanofi, personal fees from Menarini, personal fees from TEVA,

outside the submitted work; in addition, PB has 4 patents delivered (i) (EP N°3050574 *i.e.*, Use of plerixafor for treating and/or preventing acute exacerbations of chronic obstructive pulmonary disease); (ii) (EP N°20173595.8 *i.e.*, New compositions and methods of treating COVID-19 Disease); (iii) (N° WO2017203064A1 *i.e.*, MRI Method for the geometrical characterization of pulmonary airways); (iv) (N° WO2021018439A1 *i.e.*, Method for generating a biomarker system). All other authors declare they have no competing interests.

Abstract

Background: Chronic obstructive pulmonary disease (COPD) is a prevalent respiratory disease lacking effective treatment. Focusing on young COPD should help to discover disease modifying therapies. We aimed to examine the role of the CXCL12/CXCR4 axis in young COPD from both human samples and murine models.

Methods: Blood samples and lung tissues of young COPD patients and controls were obtained in order to analyse CXCL12 and CXCR4 levels. To generate a young COPD model, ten-week-old mice were exposed to cigarette smoke (CS) for 10 weeks and intranasal instillations of polyinosinic–polycytidylic acid (poly(I:C)) for the last 5 weeks to mimic exacerbations.

Results: Exposed mice presented mild airway obstruction, peri-bronchial fibrosis and right heart thickening. CXCR4 expressing cells number was increased in the blood of exposed mice, as well as in the blood of patients with COPD. Lung CXCL12 expression was higher in both exposed mice and young COPD patients. The density of fibrocytes expressing CXCR4 was increased in the bronchial submucosa of exposed mice. Conditional inactivation of CXCR4 at adult stage as well as pharmacological inhibition of CXCR4 with plerixafor injections improved lung function, reduced inflammation and protected against CS and poly-(I:C)-induced airway and cardiac remodelling. CXCR4$^{-/-}$ and plerixafor-treated mice also had less CXCR4-expressing circulating cells and a lower density of peri-bronchial fibrocytes.

Conclusions: We demonstrate that targeting CXCR4 has beneficial effects in an animal model of young COPD and provide a framework to translate these preclinical findings to clinical settings in a drug repurposing approach.

Key words: fibrocytes, bronchial remodelling, inflammation, obstruction, animal model

Abbreviations

BAL	Broncho-alveolar lavage
bFGF	basic Fibroblast Growth Factor
BSM	Bronchial smooth muscle
CS	Cigarette smoke
CT	Computed tomographic
ECG	Electrocardiogram
FEV1	Forced expiratory volume in 1 second
FEV0.05	Forced expiratory volume in 0.05 second
FVC	Forced vital capacity
IFN	Interferon
LV + S	Left ventricle plus septum
MRI	Magnetic Resonance Imaging
Poly-(I:C)	Polyinosinic–polycytidylic acid
RA	Room air
RV	Right ventricle
RVSP	Right ventricular systolic pressure
VEGF	Vascular Endothelial Growth Factor

Introduction

Chronic obstructive pulmonary disease (COPD) is a common disease, characterized by persistent respiratory symptoms and airflow limitation [1]. Major risk factors for COPD include chronic exposure to noxious particles, mainly cigarette smoke (CS), and airway infections [2]. Young COPD has been recently defined as patients aged <50 years, with a smoking exposure >10 pack-years, and a ratio between forced expiratory volume in 1 second (FEV1) and forced vital capacity (FVC) less than 70% [1, 3]. Therapeutic interventions in young COPD patients could help to tackle the disease before reaching irreversible tissue damage [3]. However, it is extremely difficult to enrol those patients into trials and collect their bronchial samples, since they are rarely diagnosed, demonstrating the urgent need to develop animal models of young COPD.

Exposure of lung structural and immune cells to CS and infectious agents results in the release of various inflammatory substances, including chemokines [4]. The chemokine receptor CXCR4 and its associated ligand CXCL12 appear to be attractive therapeutic targets for young COPD since (i) they are implicated in the migration of inflammatory cells in COPD lungs [5], (ii) their expression and function are controlled by other cytokines [6], oxygen concentration [7] and microbial agents [8, 9], which are disrupted in COPD, and (iii) pharmacological blockade of CXCR4 reduces emphysema development in a long-term COPD murine model [10]. CXCR4 is notably expressed by fibrocytes, a rare population of circulating fibroblast-like cells [11], that are assumed to play a crucial role in COPD [5, 12].

In the present study, we thus hypothesized that the CXCL12/CXCR4 axis plays a role in the pathological processes leading to COPD development during early adulthood and, hence, that inhibiting CXCR4 would protect from CS-induced airflow limitation and tissue remodelling. In a murine model of young COPD, as well as young COPD patients' samples, both CXCR4-expressing cells in the blood and CXCL12 in the lung were upregulated. Using transgenic mice

deficient for CXCR4 or the CXCR4 antagonist plerixafor, we showed that lungs were protected against CS-induced both lung function alteration and fibrocytes accumulation, and that the right heart was resistant to cardiac remodelling.

Some of these findings have been previously reported in abstract form [13, 14].

Methods

Complete details of methods are included in the supplementary material.

Study Population

Blood samples of COPD patients were obtained from the "COBRA" cohort (Table S1) and human lung tissues from both the "Fibrochir" study (NCT01692444) [12] and "TUBE" (*i.e.*, TissUs Bronchiques et PulmonairEs, sponsored by the University hospital of Bordeaux) biological collection (Tables S2 and S3). According to the French law and the MR004 regulation, patients received an information form, allowing them to refuse the use of their surgical samples for research. Research was conducted according to the principles of the World Medical Association Declaration of Helsinki. The studies received approval from the local and national ethics committees.

Mouse model of young COPD

All animal studies were performed according to European directives for the protection of vertebrate animals and to the Declaration of Helsinki conventions for the use and care of animals. Agreement was obtained from French authorities (number A33-063-907) and all the protocols were approved by the local ethics committee.

Ten-week-old mice were exposed for 10 weeks (whole-body) to either room air (RA) or CS, as described by Almolki *et al*. [15]. After 5 weeks of CS exposure, 50 µg of poly(I:C) or its vehicle control was administered twice per week for 5 weeks via nasal aspiration.

CXCR4 genetic deletion was induced by tamoxifen. CXCR4 pharmacological inhibition was induced by subcutaneous injection of 1 mg/kg plerixafor, 5 times/week during the last 5 weeks of the protocol.

Statistical Analysis

Statistical significance, defined as $P < 0.05$, was assessed by t-tests and ANOVA for variables with parametric distribution, and by Kruskal-Wallis with multiple comparison z tests, Mann-Whitney tests, Wilcoxon tests and Spearman correlation coefficients for variables with non-parametric distribution.

Results

Chronic CS and poly(I:C) exposure induces functional obstruction, lung inflammation and both lung and heart tissue remodelling in mice

To model young COPD, we used mice at the beginning of adulthood (10-week old) [16], which are exposed to a combination of CS exposure and intranasal instillations of poly(I:C) in order to mirror the effects of smoking and exacerbations [17]. CS exposure for 5 weeks combined with 4 doses of poly(I:C) were not sufficient to trigger functional airway obstruction (Figure S1a-d). In contrast, 10 weeks of CS exposure with 10 repeated instillations of poly(I:C) during the last 5 weeks, significantly decreased the FEV0.05/FVC ratio (Figure 1a-c). Other lung function parameters, in particular respiratory system compliance and tissue elastance, were not modified by CS and poly(I:C) exposure (Figure S1e-j). At the end of the protocol, the weight gain of the exposed mice was significantly different from that of the control mice (Figure S2a-b). CS and poly(I:C) exposure increased total cell count in the BAL fluid, as well as the absolute neutrophil, lymphocyte and macrophage numbers, 1 day after the last poly(I:C) instillation (Figure 1d-f). Although lower, the increase in neutrophils and lymphocytes persisted 4 days after the last poly(I:C) instillation (Figure 1d-f). CS and poly(I:C) synergistically enhanced airflow obstruction and BAL inflammation (Figure S3). We also analysed lung proteomics obtained 1 day after the last poly-IC instillation. Of the 137 pathways that were significantly different in young COPD vs control mice, largest upregulated genes were those of the hypercytokinemia/ hyperchemokinemia box and of the pathogenesis of influenza and interferon (IFN) signalling (Figure 1g-h). In contrast, inhibited pathways were the wound healing and the xenobiotic metabolism PXR signalling pathways (Figure 1g-h).Exposed mice had a moderate but significant increase in peri-bronchial fibrosis compared to control mice (Figure 1i-j), mimicking the thickening of distal airway tissue in COPD patients [18].

Then, we investigated the impact of CS and poly(I:C) exposure on cardiac function. There was no evidence of heart failure in our model (Figure S4a-b). Moreover, there was no sign of heart rhythm disorder as assessed by ECG monitoring (Figure S4c and S5a-f). Using MRI, we also found that CS and poly(I:C)-exposition did not alter RV or LV volumes (Figure S4d-f). However, we detected a significant increase of RV wall thickness in exposed mice, indicating RV hypertrophy (Figure 1k-l). This finding was confirmed by the measurement of the Fulton index (Figure 1m). Of note, the RV systolic pressure (RVSP) did not differ between young COPD and control mice (Figure 1n).

CXCR4 and CXCL12 expression is increased in blood and lung, respectively, in experimental young COPD and in patients with COPD

We next investigated the expression of CXCR4 and CXCL12 in blood and lung of mice and humans. The percentage of CXCR4-expressing cells was significantly increased in the blood of CS and poly(I:C)-exposed mice compared to control mice, 1 day after the last poly(I:C) instillation (Figure 2a-b). This effect appeared to be due to a synergy between CS and poly(I:C) (Figure S6). The level of $CXCR4^{+}$ circulating cells decreased and became similar between control and exposed mice 4 days after the last poly(I:C) instillation (Figure 2b). No significant modification of CXCL12 plasma concentration was evidenced in mice (Figure 2c). The percentage of CXCR4-expressing cells was not significantly altered in whole lung homogenates in experimental young COPD (Figure 2d-e). However, CS and poly(I:C)-exposure significantly increased CXCL12 protein levels in lung homogenates, compared to control mice, 1 and 4 days after the last poly(I:C) instillation (Figure 2f).

To analyse the relevance of our findings to human disease, we determined whether CXCR4 expression was altered in patients with COPD by interrogating RNAseq data from whole blood of

control subjects and COPD patients (GSE100153 data set, http://www.ncbi.nlm.nih.gov/geo/). CXCR4 was significantly increased, at the mRNA level, in whole blood from patients with COPD compared to control subjects (Figure 2g). In a separate cohort of moderate to mild COPD patients (GOLD I to II, as defined by [1], Table S1), the percentage of CXCR4-expressing cells was also increased in the blood of moderate COPD patients in comparison with mild COPD patients (Figure 2h-i). In the lung, CXCR4 level was not significantly altered in patients with COPD compared to control smokers at the mRNA level (GSE76925 data set, Figure 2j), which was corroborated by a similar result at the protein level (Figure 2k-l) in a separate cohort of patients with and without COPD (Table S2). In good agreement with our findings in mouse lungs, we also found a significant increased CXCL12 expression in patients with COPD (GSE76925 data set, Figure 2m), although we were not able to confirm it at the protein level (Figure 2n). In both mouse and human lungs (Table S3), CXCL12 was predominantly localized to bronchial epithelial cells and peri-bronchial infiltrating cells, which are likely immune cells (Figure 2o-p). The CXCL12 immunostaining was markedly increased in lungs of animals exposed to CS and poly-(I:C) and lungs of patients with young COPD in comparison to control lungs. CXCR4 was similarly expressed in COPD and control patients, mainly in inflammatory cells (Figure S7a-b).

Fibrocytes and CXCR4^{+} fibrocytes are increased in lungs of experimental young COPD

The percentage of fibrocytes, defined as cells expressing CD45 and a high level of FSP1 ("CD45^{+} FSP1^{high}") [19], was significantly increased in CS and poly(I:C)-exposed lungs, 1 day after the last poly(I:C) instillation (Figure 3a-c). The average percentage of leukocytes (CD45^{+} cells) in control and exposed lungs was 69.2 % and 74.0 %, respectively (p=0.07, Figure 3d). In control and experimental young COPD, a vast majority of lung fibrocytes expressed CXCR4

(96.1 and 96.6 %, respectively, Figure 3b) and the percentage of CXCR4^{+} fibrocytes was also significantly increased in the lungs of exposed mice (Figure 3c). Four days after the last poly(I:C) instillation, the total level of fibrocytes decreased and became similar between control and experimental young COPD lungs (Figure 3c). Since the flow cytometry approach limits our analysis to the whole lung, we co-stained FSP1 with CD45 in murine lungs, 4 days after the last poly(I:C) instillation (Figure 3f) using immunohistochemistry. Similarly to what we previously reported in human lung [12], the density of peri-bronchial fibrocytes was higher in CS and poly(I:C)-exposed mice lungs than in control mice (Figure 3g). Moreover, we also observed *in situ* CXCR4-expressing fibrocytes in peri-bronchial areas of human lung samples (Figure 3h). Of note, fibrocytes were found in right and left ventricles, but their densities were unchanged by CS and poly(I:C) exposure (Figure S8).

CXCR4 deletion protects against functional airway obstruction, lung and heart tissue remodelling, and inhibits fibrocyte recruitment into the lungs in experimental young COPD

As mice genetically deficient for CXCR4 die perinatally [20], we generated conditional CXCR4 mutants using floxed allele [21] and a Cre2ERT2 strain [22], thereby obtaining mutants harbouring a specific inactivation of CXCR4 at young adulthood after tamoxifen treatment. Intraperitoneal tamoxifen administration, for 5 consecutive days, in CXCR4$^{lox/lox}$/Cre2ERT2 mice was not sufficient to induce a large CXCR4 downregulation, in particular in the lungs (Figure S9a-b). Therefore, we combined intraperitoneal tamoxifen administration and feeding mice with tamoxifen-containing food to obtain robust decrease in CXCR4 expression in the lung and bone marrow (Figure S9c-e). As tamoxifen-containing food reduced weight gain in mice (Figure S2c-d), we used CXCR4$^{lox/lox}$ mice as control mice, and gave all transgenic mice tamoxifen-containing food.

CXCR4$^{lox/lox}$/Cre2ERT2 and CXCR4$^{lox/lox}$ mice were exposed to CS and poly(I:C) for 10 weeks (Figure 4a). As expected, CXCR4 expression decreases in the lung and blood of CXCR4$^{lox/lox}$/Cre2ERT2 mice (Figure S10). Moreover, FEV0.05/FVC ratio was higher in CXCR4$^{-/-}$ mice compared to CXCR4$^{lox/lox}$ mice, when exposed to CS and poly(I:C) (Figure 4b). In the BAL fluid, CXCR4 deletion induced a significant decrease of macrophage and increase of neutrophil percentages, 1 day after the last poly(I:C) instillation (Figure 4c-e). CXCR4$^{-/-}$ mice had a significant reduction in collagen deposition around small airways, compared to CS and poly(I:C)-exposed CXCR4$^{+/+}$ mice (Figure 4f-g), confirming an important role of CXCR4 in CS-induced bronchial remodelling.

We then assessed the impact of CXCR4 deletion on right heart remodelling. CXCR4 deletion did not affect hemodynamic and electrophysiological properties (Figure S11 and S5g-l) but it significantly reduced the RV wall thickness as assessed by heart MRI *in vivo* and the Fulton index *ex vivo* in exposed mice (Figure 4h-j). RVSP value was unchanged by CXCR4 deletion (Figure 4k).

Moreover, we observed reduced flow cytometry levels of CXCR4^{+} fibrocytes in CS and poly(I:C)-exposed whole lungs of CXCR4$^{-/-}$ mice compared with CXCR4$^{+/+}$ exposed mice, 1 day after the last poly(I:C) instillation (Figure 5a-d). Four days after the last poly(I:C) instillation, the density of fibrocytes was also significantly decreased around the small airways (Figure 5f-g).

Pharmacological inhibition of CXCR4 protects against functional obstruction and inhibits fibrocyte recruitment into the lungs in experimental COPD

We then assessed the efficacy of a CXCR4 antagonist (*i.e.* AMD3100, plerixafor) in the young COPD murine model (Figure 6a). Mice weight was not affected by daily subcutaneous plerixafor treatment during the second half of the protocol (Figure S2e-f). Plerixafor significantly reduced

CXCR4 expression 1 day after the last poly(I:C) instillation in circulating cells, but not in lung cells (Figure S12). In exposed-mice treated with plerixafor, the FEV0.05/FVC ratio was significantly higher than vehicle-treated exposed mice (Figure 6b). The total number of cells in the BAL fluid and its composition was unchanged by plerixafor treatment (Figure 6c-e). The peri-bronchial fibrosis was significantly decreased in the lungs of plerixafor-treated exposed mice (Figure 6f-g). To identify pathways that were differentially regulated by the young COPD protocol and plerixafor treatment, we performed proteome analysis on lungs obtained 1 day after the last poly-IC instillation. Comparison analysis revealed a significant inhibition of pathways of inflammation, cell invasion, movement, adhesion and synthesis of reactive oxygen species (ROS) in relation to plerixafor treatment (Figure 6h). These changes were driven by down-regulation of a core set of proteins such as thioredoxin interacting protein (TXNIP), matrix metalloproteinase-8 (MMP-8) and vimentin (Figure S13).

Treatment with plerixafor also reduced the development of RV hypertrophy in exposed mice (Figure 6i). The RVSP, as well as heart electrophysiological properties remained unchanged by CXCR4 inhibition (Figure 6j, S5m-r).

Flow cytometry 1 day after the last poly(I:C) instillation showed a significant decrease of the numbers of both fibrocytes and $CXCR4^{+}$ fibrocytes in the lungs of exposed mice by plerixafor (Figure S14a-e). 4 days after the last poly(I:C) instillation, the density of peri-bronchial fibrocytes identified by immunohistochemistry was significantly reduced by plerixafor (Figure S14f-g).

Discussion

Taken together, our data demonstrate that the CXCL12/CXCR4 axis plays a major role in the pathogenesis of lung and heart remodelling of young COPD. Indeed, both genetic silencing and pharmacological inhibition of CXCR4 in our experimental young COPD model reduced both the level of CXCR4-expressing cells in the peripheral circulation and fibrocyte recruitment into the lungs, along with a proteomic signature consistent with decreased inflammation. As a consequence, CXCR4 inhibition prevented airflow limitation and lung and cardiac remodelling. For translational purpose, we also showed that $CXCR4^{+}$-cells were increased in the blood of patients with a mild COPD whereas CXCL12 was increased in the lung of young COPD patients.

We designed the present dedicated murine model of young COPD to examine pathophysiological processes at the onset of the disease. Instead of deciphering the relative contribution of CS and poly-(I:C), this study aims at developing and using a young COPD model, based on the following: first, 10-week old mice exposed to CS for 10 weeks would correspond to young human adults chronically exposed to tobacco smoke for several years [16], and poly-(I:C) administration mimics exacerbations occurring in young COPD a frequency similar to the COPD population [17]. Second, as in humans, exposed mice exhibited limited but significant airflow limitation together with both neutrophilic/lymphocytic airway inflammation and distal airway remodelling, without obvious signs of alveolar destruction, allowing our design to model the bronchial component of COPD [23]. By contrast, the vast majority of murine COPD models are based on long-term CS exposure (up to 6 months) either mimicking emphysema, or reproducing severe airway obstruction together with emphysema-like changes [24]. Moreover, we used a combination of CS exposure with poly-(I:C) to mimic respiratory viral infections [25], which are more frequent in smokers [26] and young COPD [17]. The present model also includes features

of early RV hypertrophy [27], without established pulmonary hypertension, as previously identified in a long term murine model [28], thus confirming again the relevance of this animal model of young COPD. Cardiovascular diseases, are indeed frequently seen in current smokers [29] and patients with COPD [30], including young COPD [31].

A main result of the present study is the increase of CXCL12 expression in the lungs of young COPD mice and patients, along with an increase in $CXCR4^{+}$-cells in the blood of young COPD mice as well as in COPD patients. Treating mice with the CXCR4 antagonist plerixafor prevented the increase of $CXCR4^{+}$-cells, attenuated tissue fibrocytes recruitment and lung function degradation. Targeting CXCR4 with daily injections of plerixafor during the 5 last weeks of the protocol as well as genetic deletion of CXCR4 also decreased CS and poly-(I:C) induced-right heart remodelling. In this connection, neutralizing CXCL12 or antagonizing CXCR4 has been previously shown to attenuate RV hypertrophy in a rat model of severe pulmonary hypertension [32]. The beneficial effect of plerixafor on lung function and remodelling in exposed mice, exhibiting increased CXCR4 solely in the blood, was similar with that observed in $CXCR4^{-/-}$ mice. This suggests that such beneficial effects occurred through CXCR4 reduction in the blood rather than in the lungs. These results are in agreement with findings obtained in mice treated with another CXCR4 antagonist or with CXCL12 neutralizing antibodies, in the context of pulmonary fibrosis, where reduction of fibrocytes accumulation concomitantly improved lung outcomes [11, 33]. The reduction of tissue fibrocytes could thus contribute to lower chronic inflammation [34]. Finally, plerixafor-induced increased mobilization of hematopoietic progenitor cells from the bone marrow may also participate in the improvement of lung function and remodelling [10]. Several mechanisms of up-regulation of blood $CXCR4^{+}$-cells may be proposed, including effects mediated by mild/intermittent hypoxia [7], the Vascular Endothelial

Growth Factor (VEGF) et the basic Fibroblast Growth Factor (bFGF), described in endothelial cells [35], or IL-33, described in fibrocytes [36, 37].

Acknowledgments

We thank the study participants and the staff of the Thoracic Surgery, Radiology, Pathology, Respiratory, Lung Function Testing departments from the University Hospital of Bordeaux (Bordeaux, France), Fabienne Estella for technical assistance with mice protocol, Isabelle Goasdoue, Isabelle Bernis, Natacha Robert, Virginie Niel, and Marine Servat from the clinical investigation center for technical assistance, and Atika Zouine and Vincent Pitard for technical assistance at the Flow cytometry facility (CNRS UMS 3427, INSERM US 005, Univ. Bordeaux, F-33000 Bordeaux, France), Anne-Aurélie Raymond for help with proteomic analysis at the Oncoprot Platform (TBMCore US005). Christel Poujol, Sébastien Marais and Fabrice Cordelières for help with imaging and image analysis et the Bordeaux Imaging Centre (BIC; Bordeaux, France). Microscopy was performed at BIC, a service unit of the CNRS-INSERM and Bordeaux University, a member of the national BioImaging infrastructure of France supported by the French National Research Agency (ANR-10-INBS-04).

Funding: the project was supported by a grant from the “Fondation de l’Université de Bordeaux” (Fonds pour les maladies chroniques nécessitant une assistance médico-technique FGLMR/AVAD) (ID), a grant from « Aquitaine Science Transfert » (PB) and AstraZeneca (an unrestricted grant to PB), the “Investments in the Future” program managed by the “Agence Nationale de la Recherche” (ANR, grant reference ANR-10-IAHU-04). The COBRA cohort was funded by AstraZeneca, Chiesi, Glaxo-SmithKline, Novartis, Chiesi,Roche and Legs Poix fondation.

References

1. Global Initiative for Chronic Obstructive Lung Disease [Internet]. Global Initiative for Chronic Obstructive Lung Disease - GOLD [cited 2023 Feb 6].Available from: https://goldcopd.org/.

2. Mannino DM, Buist AS. Global burden of COPD: risk factors, prevalence, and future trends. *Lancet* 2007; 370: 765–773.

3. Martinez FJ, Agusti A, Celli BR, Han MK, Allinson JP, Bhatt SP, Calverley P, Chotirmall SH, Chowdhury B, Darken P, Da Silva CA, Donaldson G, Dorinsky P, Dransfield M, Faner R, Halpin DM, Jones P, Krishnan JA, Locantore N, Martinez FD, Mullerova H, Price D, Rabe KF, Reisner C, Singh D, Vestbo J, Vogelmeier CF, Wise RA, Tal-Singer R, Wedzicha JA. Treatment Trials in Young Patients with Chronic Obstructive Pulmonary Disease and Pre-Chronic Obstructive Pulmonary Disease Patients: Time to Move Forward. *Am J Respir Crit Care Med* 2022; 205: 275–287.

4. Henrot P, Prevel R, Berger P, Dupin I. Chemokines in COPD: From Implication to Therapeutic Use. *Int J Mol Sci* 2019; 20.

5. Dupin I, Allard B, Ozier A, Maurat E, Ousova O, Delbrel E, Trian T, Bui H-N, Dromer C, Guisset O, Blanchard E, Hilbert G, Vargas F, Thumerel M, Marthan R, Girodet P-O, Berger P. Blood fibrocytes are recruited during acute exacerbations of chronic obstructive pulmonary disease through a CXCR4-dependent pathway. *J. Allergy Clin. Immunol.* 2016; 137: 1036-1042.e7.

6. Busillo JM, Benovic JL. Regulation of CXCR4 signaling. *Biochimica et Biophysica Acta (BBA) - Biomembranes* 2007; 1768: 952–963.

7. Schioppa T, Uranchimeg B, Saccani A, Biswas SK, Doni A, Rapisarda A, Bernasconi S, Saccani S, Nebuloni M, Vago L, Mantovani A, Melillo G, Sica A. Regulation of the Chemokine Receptor CXCR4 by Hypoxia. *Journal of Experimental Medicine* 2003; 198: 1391–1402.

8. Tian X, Xie G, Xiao H, Ding F, Bao W, Zhang M. CXCR4 knockdown prevents inflammatory cytokine expression in macrophages by suppressing activation of MAPK and NF-κB signaling pathways. *Cell & Bioscience* 2019; 9: 55.

9. Petty JM, Sueblinvong V, Lenox CC, Jones CC, Cosgrove GP, Cool CD, Rai PR, Brown KK, Weiss DJ, Poynter ME, Suratt BT. Pulmonary stromal-derived factor-1 expression and effect on neutrophil recruitment during acute lung injury. *J. Immunol.* 2007; 178: 8148–8157.

10. Barwinska D, Oueini H, Poirier C, Albrecht ME, Bogatcheva NV, Justice MJ, Saliba J, Schweitzer KS, Broxmeyer HE, March KL, Petrache I. AMD3100 ameliorates cigarette smoke-induced emphysema-like manifestations in mice. *Am. J. Physiol. Lung Cell Mol. Physiol.* 2018; 315: L382–L386.

11. Phillips RJ, Burdick MD, Hong K, Lutz MA, Murray LA, Xue YY, Belperio JA, Keane MP, Strieter RM. Circulating fibrocytes traffic to the lungs in response to CXCL12 and mediate fibrosis. *J. Clin. Invest.* 2004; 114: 438–446.

12. Dupin I, Thumerel M, Maurat E, Coste F, Eyraud E, Begueret H, Trian T, Montaudon M, Marthan R, Girodet P-O, Berger P. Fibrocyte accumulation in the airway walls of COPD patients. *Eur. Respir. J.* 2019; 54.

13. Dupin I, Henrot P, Maurat E, Eyraud E, Esteves P, Zysman M, Campagnac M, Dubreuil M, Cardouat G, Bouchet C, Ousova O, Trian T, Freund-Michel V, Berger P. Targeting CXCR4 as a therapeutic strategy to improve outcomes in a mouse model of early chronic obstructive pulmonary disease (COPD). *ERJ Open Research* [Internet] European Respiratory Society; 2022 [cited 2023 Feb 6]; 8Available from: https://openres.ersjournals.com/content/8/suppl_8/9.

14. Dupin I, Dubreuil M, Freund-Michel V, Maurat E, Campagnac M, Ousova O, Trian T, Girodet P-O, Berger P. Targeting CXCR4 as a therapeutic strategy to improve outcomes in a mouse model of early chronic obstructive pulmonary disease (COPD). *ERJ Open Research* [Internet] European Respiratory Society; 2019 [cited 2023 Feb 6]; 5Available from: https://openres.ersjournals.com/content/5/suppl_2/PP225.

15. Almolki A, Guenegou A, Golda S, Boyer L, Benallaoua M, Amara N, Bachoual R, Martin C, Rannou F, Lanone S, Dulak J, Burgel P-R, El-Benna J, Leynaert B, Aubier M, Boczkowski J. Heme oxygenase-1 prevents airway mucus hypersecretion induced by cigarette smoke in rodents and humans. *Am J Pathol* 2008; 173: 981–992.

16. Dutta S, Sengupta P. Men and mice: Relating their ages. *Life Sciences* 2016; 152: 244–248.

17. Cosío BG, Casanova C, Soler-Cataluña JJ, Soriano JB, García-Río F, de Lucas P, Alfageme I, Rodríguez González-Moro JM, Sánchez G, Ancochea J, Miravitlles M. Unravelling young COPD and pre-COPD in the general population. *ERJ Open Res* 2023; 9: 00334–02022.

18. Hogg JC, McDonough JE, Sanchez PG, Cooper JD, Coxson HO, Elliott WM, Naiman D, Pochettino M, Horng D, Gefter WB, Wright AC. Micro–Computed Tomography Measurements of Peripheral Lung Pathology in Chronic Obstructive Pulmonary Disease. *Proc Am Thorac Soc* 2009; 6: 546–549.

19. Sangaletti S, Tripodo C, Cappetti B, Casalini P, Chiodoni C, Piconese S, Santangelo A, Parenza M, Arioli I, Miotti S, Colombo MP. SPARC oppositely regulates inflammation and fibrosis in bleomycin-induced lung damage. *Am J Pathol* 2011; 179: 3000–3010.

20. Tachibana K, Hirota S, Iizasa H, Yoshida H, Kawabata K, Kataoka Y, Kitamura Y, Matsushima K, Yoshida N, Nishikawa S, Kishimoto T, Nagasawa T. The chemokine receptor CXCR4 is essential for vascularization of the gastrointestinal tract. *Nature* 1998; 393: 591–594.

21. Tokoyoda K, Egawa T, Sugiyama T, Choi B-I, Nagasawa T. Cellular Niches Controlling B Lymphocyte Behavior within Bone Marrow during Development. *Immunity* 2004; 20: 707–718.

22. Jullien N, Goddard I, Selmi-Ruby S, Fina J-L, Cremer H, Herman J-P. Use of ERT2-iCre-ERT2 for conditional transgenesis. *Genesis* 2008; 46: 193–199.

23. Higham A, Quinn AM, Cançado JED, Singh D. The pathology of small airways disease in COPD: historical aspects and future directions. *Respir Res* 2019; 20: 49.

24. Tanner L, Single AB. Animal Models Reflecting Chronic Obstructive Pulmonary Disease and Related Respiratory Disorders: Translating Pre-Clinical Data into Clinical Relevance. *JIN* Karger Publishers; 2020; 12: 203–225.

25. Kang M-J, Lee CG, Lee J-Y, Dela Cruz CS, Chen ZJ, Enelow R, Elias JA. Cigarette smoke selectively enhances viral PAMP- and virus-induced pulmonary innate immune and remodeling responses in mice. *J Clin Invest* 2008; 118: 2771–2784.

26. Arcavi L, Benowitz NL. Cigarette Smoking and Infection. *Archives of Internal Medicine* 2004; 164: 2206–2216.

27. Hilde JM, Skjørten I, Grøtta OJ, Hansteen V, Melsom MN, Hisdal J, Humerfelt S, Steine K. Right ventricular dysfunction and remodeling in chronic obstructive pulmonary disease without pulmonary hypertension. *J Am Coll Cardiol* 2013; 62: 1103–1111.

28. Weissmann N, Lobo B, Pichl A, Parajuli N, Seimetz M, Puig-Pey R, Ferrer E, Peinado VI, Domínguez-Fandos D, Fysikopoulos A, Stasch J-P, Ghofrani HA, Coll-Bonfill N, Frey R, Schermuly RT, García-Lucio J, Blanco I, Bednorz M, Tura-Ceide O, Tadele E, Brandes RP, Grimminger J, Klepetko W, Jaksch P, Rodriguez-Roisin R, Seeger W, Grimminger F, Barberà JA. Stimulation of soluble guanylate cyclase prevents cigarette smoke-induced pulmonary hypertension and emphysema. *Am J Respir Crit Care Med* 2014; 189: 1359–1373.

29. Banks E, Joshy G, Korda RJ, Stavreski B, Soga K, Egger S, Day C, Clarke NE, Lewington S, Lopez AD. Tobacco smoking and risk of 36 cardiovascular disease subtypes: fatal and non-fatal outcomes in a large prospective Australian study. *BMC Medicine* 2019; 17: 128.

30. Chen W, Thomas J, Sadatsafavi M, FitzGerald JM. Risk of cardiovascular comorbidity in patients with chronic obstructive pulmonary disease: a systematic review and meta-analysis. *Lancet Respir Med* 2015; 3: 631–639.

31. Divo MJ, Marin JM, Casanova C, Cabrera Lopez C, Pinto-Plata VM, Marin-Oto M, Polverino F, de-Torres JP, Billheimer D, Celli BR, Celli BR, Marin JM, Macario CC, Pinto-Plata V, de-Torres JP, Divo MJ, Lopez CC, Polverino F, Oto MM, The BODE Collaborative Group. Comorbidities and mortality risk in adults younger than 50 years of age with chronic obstructive pulmonary disease. *Respiratory Research* 2022; 23: 267.

32. Bordenave J, Thuillet R, Tu L, Phan C, Cumont A, Marsol C, Huertas A, Savale L, Hibert M, Galzi J-L, Bonnet D, Humbert M, Frossard N, Guignabert C. Neutralization of CXCL12 attenuates established pulmonary hypertension in rats. *Cardiovasc. Res.* 2019; .

33. Griffiths K, Habiel DM, Jaffar J, Binder U, Darby WG, Hosking CG, Skerra A, Westall GP, Hogaboam CM, Foley M. Anti-fibrotic Effects of CXCR4-Targeting i-body AD-114 in Preclinical Models of Pulmonary Fibrosis. *Sci Rep* 2018; 8: 3212.

34. Eyraud E, Maurat E, Sac-Epée J-M, Henrot P, Zysman M, Esteves P, Trian T, Bégueret H, Girodet P-O, Thumerel M, Hustache-Castaing R, Marthan R, Levet F, Vallois P, Contin-Bordes C, Berger P, Dupin I. Short-range interactions between fibrocytes and CD8+ T cells in COPD bronchial inflammatory response [Internet]. bioRxiv; 2022 [cited 2022 Oct 24]. p. 2022.10.21.513138Available from: https://www.biorxiv.org/content/10.1101/2022.10.21.513138v1.

35. Salcedo R, Wasserman K, Young HA, Grimm MC, Howard OM, Anver MR, Kleinman HK, Murphy WJ, Oppenheim JJ. Vascular endothelial growth factor and basic fibroblast growth factor induce expression of CXCR4 on human endothelial cells: In vivo neovascularization induced by stromal-derived factor-1alpha. *Am J Pathol* 1999; 154: 1125–1135.

36. Wang C-H, Weng C-M, Huang T-T, Lee M-J, Lo C-Y, Chen M-C, Chou C-L, Kuo H-P. Anti-IgE therapy inhibits chemotaxis, proliferation and transformation of circulating fibrocytes in patients with severe allergic asthma. *Respirology* 2021; .

37. Berger P, Dupin I. Unravelling the effects of omalizumab on fibrocytes. *Respirology* 2021; 26: 825–827.

Fig legends

Figure 1: Evaluation of lung function, inflammation, bronchial and heart remodelling in experimental COPD. a) Mice are exposed either to room air (RA) and challenged with PBS, or exposed to cigarette smoke (CS) and challenged with poly(I:C), during 10 weeks. They are sacrificed at day 68 or 71 (i.e. 1 day or 4 days after the last poly(I:C) instillation). b) Average expiratory flow-volume curves of RA+PBS-exposed mice (black curve) and CS+poly(I:C)-exposed mice (grey curve). Lower and upper error bars represent standard deviations for CS+poly(I:C) and RA+PBS-exposed mice, respectively. c) FEV0.05/FVC (FEV0.05: Forced Expiratory Volume during 0.05 s, FVC: Forced Vital Capacity) of RA+PBS-exposed mice (black circles) and CS+poly(I:C)-exposed mice (grey squares). Data represent individual mice. d) Total cell count in bronchoalveolar lavage (BAL). Kruskal-Wallis test followed by Dunn's post-tests. e-f), BAL differential cell recovery 1 day (d+1) and 4 days (d+4) after the last poly(I:C) instillation. g) Top Canonical Ingenuity Pathways significantly altered in CS+poly(I:C) (n=5) *vs* RA+PBS (n=5)-exposed lungs (n=5) obtained 1 day after the last poly-IC instillation, ranked by Z-score (negative and positive for the pathways represented respectively on the top and bottom part of the graph), obtained by Gene Set Enrichment Analysis. h) Heatmaps of differentially regulated proteins in CS+poly(I:C) vs RA+PBS-exposed lungs, from the pathways "hypercytokinemia/hyperchemokinemia in the pathogenesis of influenza" (left), "wound healing signalling pathway" (middle) and "xenobiotic metabolism PXR signalling pathway" (right). The colour scale indicates the $\log_2$ fold changes of abundance for each protein. i) Representative Masson's trichrome stainings to assess peri-bronchial fibrosis. j) Standardized fibrosis, defined as (peri-bronchial fibrosis ("PF", %) - mean PFcontrol)/standard deviation PFcontrol). The peri-bronchial fibrosis ("PF", percentage) is defined by the ratio between the area of segmented pixels in the area of analysis divided by the total peri-bronchial area. k) Representative short-axis cine

magnetic resonance images of heart at end-systolic stage (left panels) and end-diastolic stage (middle panels) in control mice (top panels) and CS and poly(I:C)-exposed mice (bottom panels). Right panels: higher magnification of RV wall. l) Wall thickness. m) Fulton index, defined as (right ventricle (RV)/ left ventricle plus septum (LV + S). n) Right ventricular systolic pressure (RVSP). c, e, f, i, l, m, n) Unpaired t test or Mann-Whitney test. *: $P<0.05$, **: $P<0.01$, ***: $P<0.001$.

Figure 2: Characterization of CXCR4 and CXCL12 expression in the blood and lung in experimental COPD and in patients with or without COPD. a-f, o) Mice are exposed either to room air (RA) and challenged with PBS, or exposed to cigarette smoke (CS) and challenged with poly(I:C), during 10 weeks. They are sacrificed at day 68 or 71 (i.e. 1 day or 4 days after the last poly(I:C) instillation). a, d, h) Upper left panels: dot plots represent representative side scatter (SSC, y-axis)-forward scatter (FSC, x-axis) graphs of circulating (a, h) and lung (f) cells. $DAPI^-$ cells, and $DAPI^-$ $CXCR4^+$ cells are shown respectively in grey and pink. Upper right panels and bottom panels: histograms represent representative cell count (y-axis) versus Phycoerythrin (PE) fluorescence (x-axis) in $DAPI^-$ circulating (a, h) and lung (d) cells. Percentages of $CXCR4^+$ cells in the $DAPI^-$ cells are shown in pink. b, e) Levels of circulating (c) and lung (h) $CXCR4^+$ cells 1 day (d+1) and 4 days (d+4) after the last poly(I:C) instillation. c, f) Plasma (c) and lung (f) CXCL12 concentration at d+1 and d+4. For lung CXCL12 concentration, the value is normalized to total protein concentration. g) CXCR4 mRNA expression in whole blood. Data are derived from a publicly available GSE-set (GSE100153). Control subjects n=24; patients with COPD n=19. i) Levels of circulating $CXCR4^+$ cells in patients with moderate COPD (GOLD I, defined by forced expiratory volume in 1 second (FEV1) ≥ 80% predicted, n=5) and mild COPD (GOLD II, defined by 50% ≤ FEV1 < 80% predicted, n=5). j, m) CXCR4 (j) and CXCL12 (m) mRNA expression in human lungs. Data are derived from a publicly available GSE-set (GSE76925). Control subjects n=40; patients with COPD n=111. k, l, n) Immunoblot assay of CXCR4 protein expression levels (k), its quantification (l) and CXCL12 levels (measured by ELISA, n) in lung samples from control subjects (n=4) and patients with COPD (n=4). Stain free gel technology has been used for loading control expression quantification. For lung CXCL12 concentration, the value is normalized to total protein concentration. o, p) Representative stainings of CXCL12 (magenta) and nucleus (blue) in peri-bronchial areas of mouse (o) and human (p) lungs. Lower

panels: higher magnification of the images surrounded by white squares in the upper panels. Images obtained in RA and PBS *vs* CS and poly(I:C)-exposed mice and in control *vs* young COPD lungs have been acquired with the same exposure time and gain. The white arrowheads and arrows indicate respectively CXCR4-expressing bronchial cells and immune-type cells. b, c, e, f, g, i, j, l, m, n) Medians are represented as horizontal lines. *: $P < 0.05$, **: $P < 0.01$, ***: $P < 0.001$, Mann-Whitney test.

Figure 3: Characterization of lung fibrocyte level and localization in experimental COPD and in patients with or without COPD. a-g) Mice are exposed either to room air (RA) and challenged with PBS, or exposed to cigarette smoke (CS) and challenged with poly(I:C), during 10 weeks. They are sacrificed 1 day ("d+1") or 4 days ("d+4") after the last poly(I:C) instillation. a) Representative flow cytometry contour plots in each condition. The x-axis is for CD45-Allophycocyanin (APC) fluorescence and the y-axis, FSP1-Fluorescein-5-isothiocyanate (FITC) fluorescence. Percentages of $CD45^+$ $FSP1^{high}$ cells are shown in green. b) Representative cell count (y-axis) versus CXCR4-Phycoerythrin (PE) fluorescence (x-axis) in $CD45^+$ $FSP1^{high}$-cell subsets in mouse lungs. c-e) Levels of lung $CD45^+$ $FSP1^{high}$ cells (c), $CD45^+$ cells (d), $CD45^+$ $FSP1^{high}$ $CXCR4^+$ cells (e), in RA+PBS-exposed mice (black circles) and CS+poly(I:C)-exposed mice (grey squares), at d+1 and d+4. f) Representative stainings of CD45 (green) and FSP1 (red) in peri-bronchial areas (delimited in pink) of lung mice at d+4. The white arrows indicate fibrocytes, defined as $CD45^+$ $FSP1^+$ cells. g) Quantification of fibrocyte density (normalized by peri-bronchial area). h) Representative stainings of CD45 (green) and FSP1 (red) in peri-bronchial area. The white arrowheads indicate fibrocytes, defined as $CD45^+$ $FSP1^+$ cells. f) Representative stainings of CD45 (green), FSP1 (red), nuclei (DAPI, blue) and CXCR4 (white) in peri-bronchial areas of lung samples of control subjects and patients with COPD. The white arrows indicate CXCR4-expressing fibrocytes, defined as $CD45^+$ $FSP1^+$ $CXCR4^+$ cells. f, h) Left and lower panels: higher magnification of the images surrounded by white squares in the right upper panels. c-e, g) Medians are represented as horizontal lines. *: $P < 0.05$, **: $P < 0.01$, Mann-Whitney test.

Figure 4: Evaluation of lung function, inflammation and bronchial and heart remodelling upon conditional knockout of CXCR4 in experimental COPD. a) CXCR4$^{lox/lox}$ (grey squares) and CXCR4$^{lox/lox}$/Cre2ERT2 (pink squares) mice are exposed to cigarette smoke (CS) and challenged with poly(I:C). All the mice were administered with 1 mg intraperitoneal tamoxifen for 5 consecutive days at the beginning of the COPD protocol, and then fed by tamoxifen-containing food during the remaining protocol. They are sacrificed at day 68 or 71 (1 day and 4 days after the last poly(I:C) instillation). b) FEV0.05/FVC in the different conditions. Data represent individual mice. c) Total cell count in bronchoalveolar lavage (BAL). Kruskal-Wallis test followed by Dunn's post-tests. d-e) BAL relative (d) and absolute (e) cell composition respectively 1 day and 4 days after the last poly(I:C) instillation. f) Representative Masson's trichrome stainings to assess peri-bronchial fibrosis. g) Standardized fibrosis, defined as (peri-bronchial fibrosis ("PF", %) - mean PFcontrol)/standard deviation PFcontrol). The peri-bronchial fibrosis ("PF", percentage) is defined by the ratio between the area of segmented pixels in the area of analysis divided by the total peri-bronchial area. h) Representative short-axis cine magnetic resonance images at end-systolic stage (left panels) and end-diastolic stage (middle panels) in CS and poly(IC)-exposed CXCR4$^{lox/lox}$ mice (top panels) and CS and poly(IC)-exposed CXCR4$^{lox/lox}$/Cre2ERT2 mice (bottom panels). Right panels: higher magnification of RV wall. i) Wall thickness. j) Fulton index, defined as (right ventricle (RV)/ left ventricle plus septum (LV + S). k) Right ventricular systolic pressure (RVSP). b, d, e, g, j, k) *: $P<0.05$, **: $P<0.01$, ***: $P<0.001$. Unpaired t test or Mann-Whitney test.

Figure 5: Characterization of fibrocyte level and peri-bronchial density in lung upon conditional knockout of CXCR4 in experimental COPD. $CXCR4^{lox/lox}$ (grey squares) and $CXCR4^{lox/lox}$/Cre2ERT2 (pink squares) mice are exposed to cigarette smoke (CS) and challenged with poly(I:C). They are sacrificed at day 68 or 71 (1 day and 4 days after the last poly(I:C) instillation). a) Representative flow cytometry contour plots in each condition. The x-axis is for CD45-Allophycocyanin (APC) fluorescence and the y-axis, FSP1-Fluorescein-5-isothiocyanate (FITC) fluorescence. Percentages of $CD45^+$ $FSP1^{high}$ cells are shown in green. b) Representative cell count (y-axis) versus CXCR4-Phycoerythrin (PE) fluorescence (x-axis) in $CD45^+$ $FSP1^{high}$-cell subsets in mouse lungs. c-e) Levels of lung $CD45^+$ $FSP1^{high}$ cells (c), $CD45^+$ $FSP1^{high}$ $CXCR4^+$ cells (d), $CD45^+$ cells (e) 1 day after the last poly(I:C) instillation in each condition. f) Quantification of fibrocyte density (normalized by peri-bronchial area) 4 days after the last poly(I:C) instillation in each condition. g) Representative stainings of CD45 (red) and FSP1 (green) in peri-bronchial area (delimited in pink) in each condition. The white arrows indicate fibrocytes, defined as $CD45^+$ $FSP1^+$ cells. c-f) Medians are represented as horizontal lines. *: $P < 0.05$, Unpaired t test or Mann-Whitney test.

Figure 6: Evaluation of lung function, inflammation and bronchial and heart remodelling upon pharmacological blockage of CXCR4 in experimental COPD. a) Mice are exposed to cigarette smoke (CS), challenged with poly(I:C) and treated with plerixafor ("pleri", 1 mg/kg, purple squares) or its vehicle (grey squares). They are sacrificed at day 68 or 71 (1 day and 4 days after the last poly(I:C) instillation). b) FEV0.05/FVC in the different conditions. Data represent individual mice. c) Total cell count in bronchoalveolar lavage (BAL). Kruskal-Wallis test followed by Dunn's post-tests. d-e) BAL relative (d) and absolute (e) cell composition respectively 1 day and 4 days after the last poly(I:C) instillation. f) Representative Masson's trichrome stainings to assess peri-bronchial fibrosis. g) Standardized fibrosis, defined as (peri-bronchial fibrosis ("PF", %) - mean PFcontrol)/standard deviation PFcontrol). The peri-bronchial fibrosis ("PF", percentage) is defined by the ratio between the area of segmented pixels in the area of analysis divided by the total peri-bronchial area. h) Heatmaps of significantly differentially regulated pathways identified by Ingenuity Pathway analysis (IPA; Qiagen), obtained by proteomics comparison of CS+poly(I:C) (n=5) *vs* RA+PBS (n=5)-exposed lungs (n=5) (all treated by vehicle), and plerixafor (n=5) vs vehicle (n=5)-treated lungs (all exposed to CS+poly(I:C)). The colour scale indicates the Z-score value. i) Fulton index, defined as (right ventricle (RV)/ left ventricle plus septum (LV + S). j) Right ventricular systolic pressure (RVSP). b, d, e, g, i, j) *: $P<0.05$, **: $P<0.01$, ***: $P<0.001$. Unpaired t test or Mann-Whitney test.

Figure 1

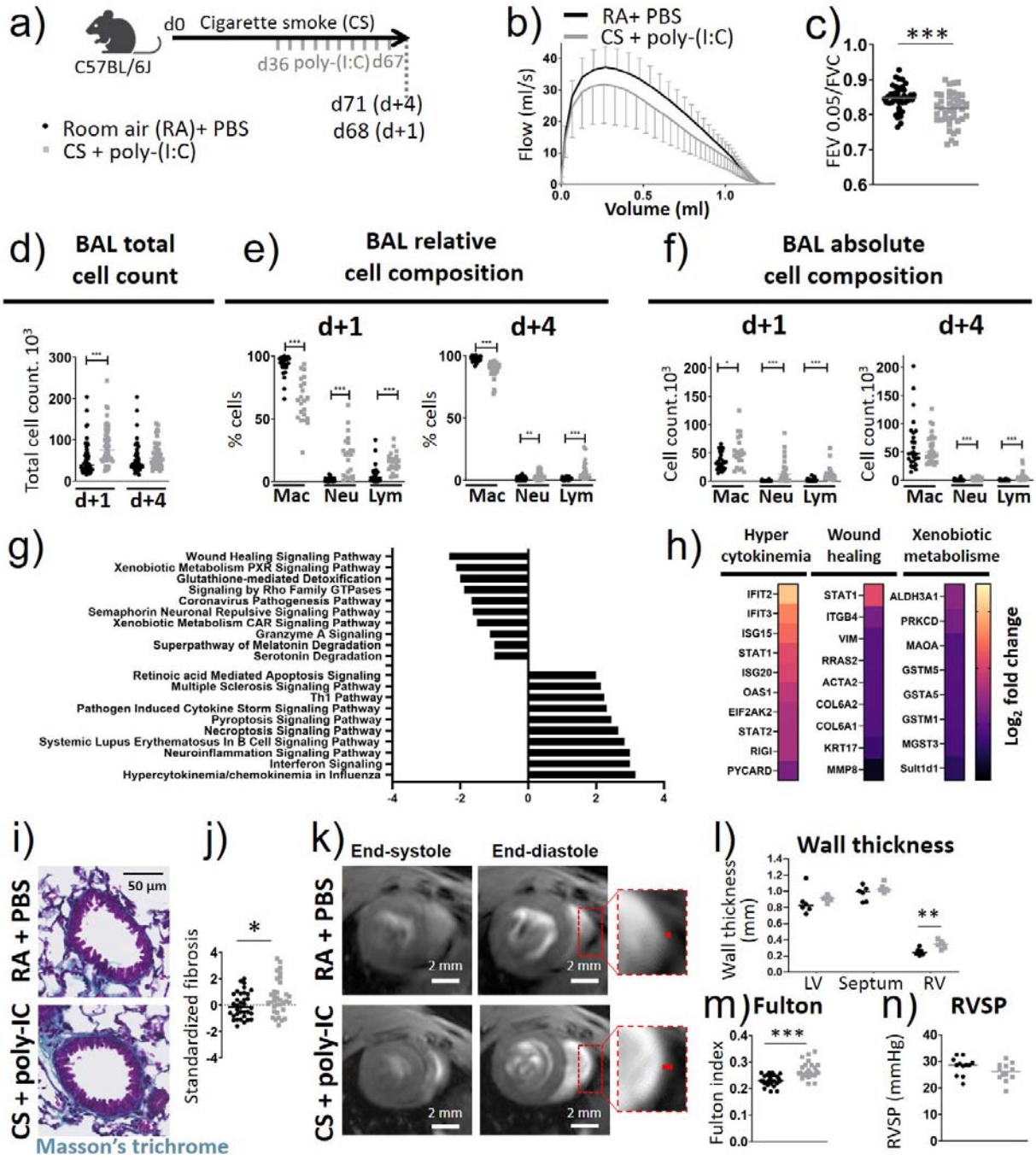
a)
C57BL/6J
d0 Cigarette smoke (CS)
d36 poly-(I:C) d67
d71 (d+4)
d68 (d+1)
Room air (RA)+ PBS
CS + poly-(I:C)
b)
RA+ PBS
CS + poly-(I:C)
Flow (ml/s)
Volume (ml)
c)
FEV 0.05/FVC
d) BAL total cell count
Total cell count. 10³
d+1
d+4
e) BAL relative cell composition
% cells
Mac
Neu
Lym
f) BAL absolute cell composition
Cell count.10³
g)
Wound Healing Signaling Pathway
Xenobiotic Metabolism PXR Signaling Pathway
Glutathione-mediated Detoxification
Signaling by Rho Family GTPases
Coronavirus Pathogenesis Pathway
Semaphorin Neuronal Repulsive Signaling Pathway
Xenobiotic Metabolism CAR Signaling Pathway
Granzyme A Signaling
Superpathway of Melatonin Degradation
Serotonin Degradation
Retinoic acid Mediated Apoptosis Signaling
Multiple Sclerosis Signaling Pathway
Th1 Pathway
Pathogen Induced Cytokine Storm Signaling Pathway
Pyroptosis Signaling Pathway
Necroptosis Signaling Pathway
Systemic Lupus Erythematosus In B Cell Signaling Pathway
Neuroinflammation Signaling Pathway
Interferon Signaling
Hypercytokinemia/chemokinemia in Influenza
h)
Hyper cytokinemia
Wound healing
Xenobiotic metabolisme
IFIT2
IFIT3
ISG15
STAT1
ISG20
OAS1
EIF2AK2
STAT2
RIGI
PYCARD
STAT1
ITGB4
VIM
RRAS2
ACTA2
COL6A2
COL6A1
KRT17
MMP8
ALDH3A1
PRKCD
MAOA
GSTM5
GSTA5
GSTM1
MGST3
Sult1d1
Log₂ fold change
i)
50 µm
RA + PBS
CS + poly-IC
Masson's trichrome
j)
Standardized fibrosis
k)
End-systole
End-diastole
RA + PBS
CS + poly-IC
2 mm
l)
Wall thickness
Wall thickness (mm)
LV
Septum
RV
m) Fulton
Fulton index
n) RVSP
RVSP (mmHg)

Figure 2

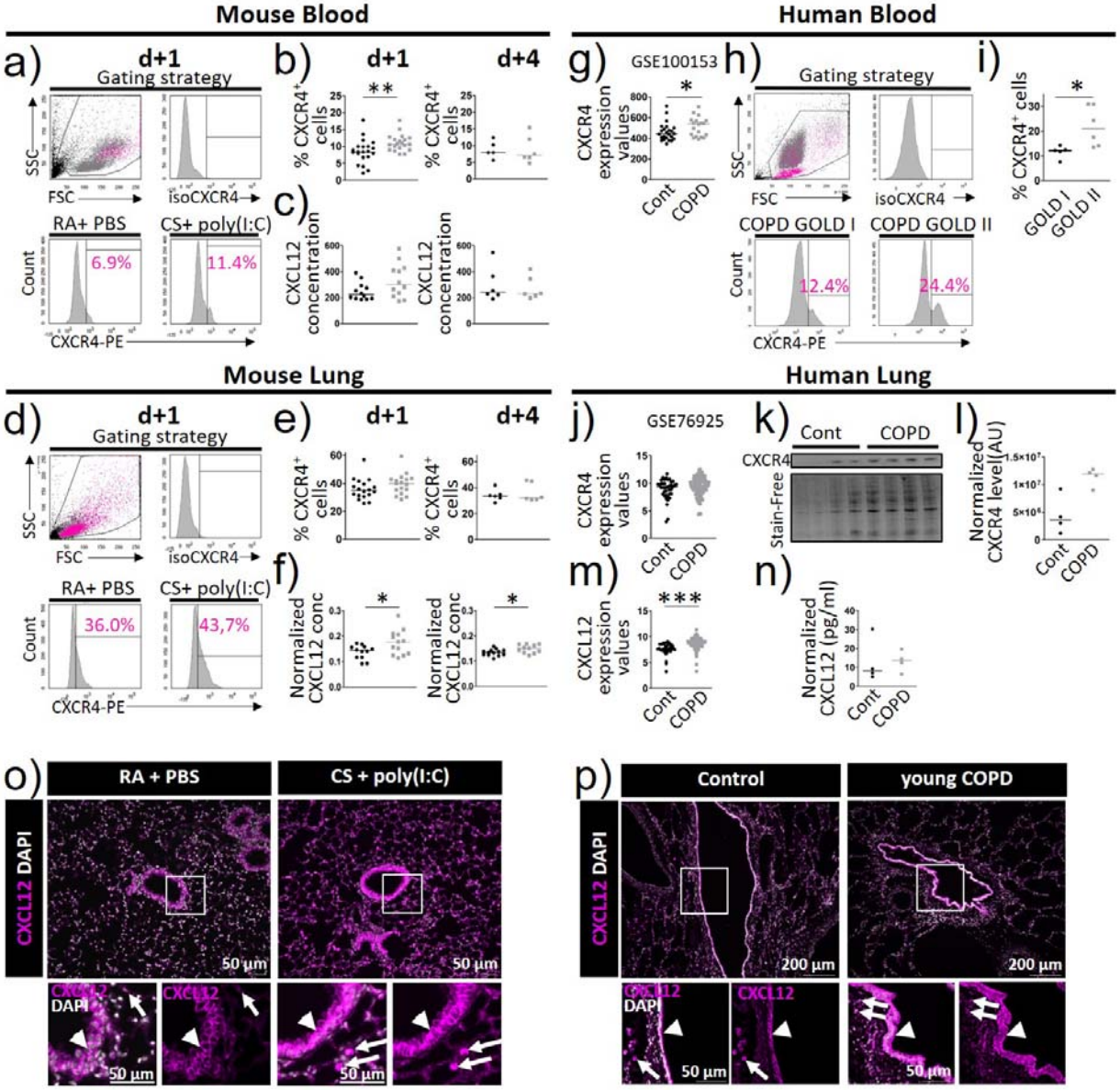
Mouse Blood
Human Blood
a)
d+1
Gating strategy
SSC
FSC
isoCXCR4
RA+ PBS
CS+ poly(I:C)
Count
6.9%
11.4%
CXCR4-PE
b)
d+1
d+4
% CXCR4+ cells
**
c)
CXCL12 concentration
g)
GSE100153
CXCR4 expression values
*
Cont
COPD
h)
COPD GOLD I
COPD GOLD II
12.4%
24.4%
i)
% CXCR4+ cells
GOLD I
GOLD II
Mouse Lung
Human Lung
d)
36.0%
43,7%
e)
f)
Normalized CXCL12 conc
***
j)
GSE76925
k)
CXCR4
Stain-Free
l)
Normalized CXCR4 level(AU)
m)
n)
Normalized CXCL12 (pg/ml)
o)
RA + PBS
CS + poly(I:C)
CXCL12 DAPI
50 µm
p)
Control
young COPD
200 µm

Figure 3

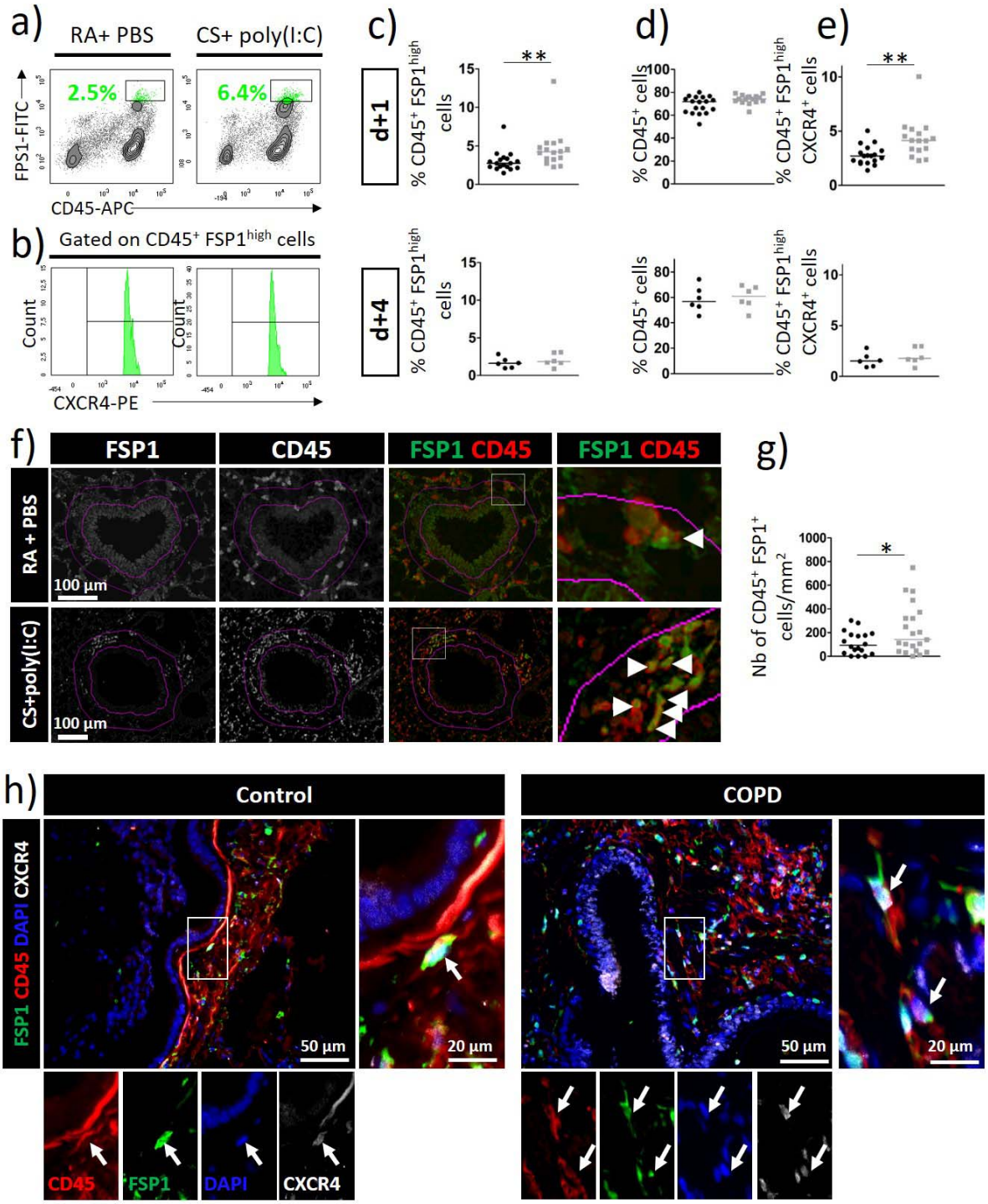
a)
RA+ PBS
CS+ poly(I:C)
2.5%
6.4%
FPS1-FITC
CD45-APC
b)
Gated on CD45+ FSP1high cells
Count
CXCR4-PE
c)
d+1
d+4
% CD45+ FSP1high cells
**
d)
% CD45+ cells
e)
% CD45+ FSP1high CXCR4+ cells
f)
FSP1
CD45
FSP1 CD45
RA + PBS
CS+poly(I:C)
100 µm
g)
Nb of CD45+ FSP1+ cells/mm2
*
h)
Control
COPD
FSP1 CD45 DAPI CXCR4
50 µm
20 µm
CD45
FSP1
DAPI
CXCR4

Figure 4

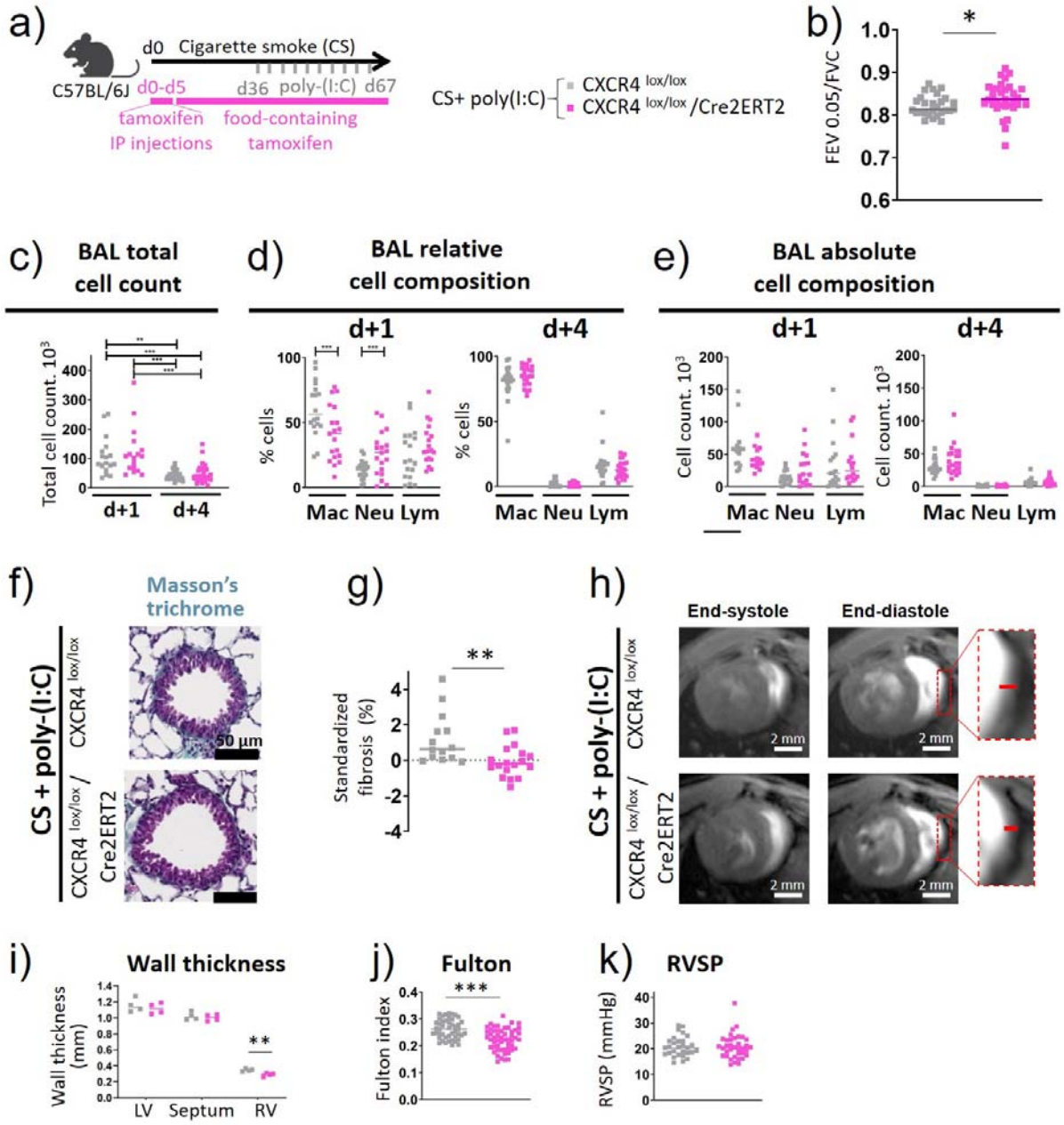
a)
C57BL/6J
d0 Cigarette smoke (CS)
d0-d5
d36 poly-(I:C) d67
tamoxifen IP injections
food-containing tamoxifen
CS+ poly(I:C)
CXCR4 lox/lox
CXCR4 lox/lox /Cre2ERT2
b)
FEV 0.05/FVC
c) BAL total cell count
Total cell count. 10³
d+1
d+4
d) BAL relative cell composition
% cells
Mac Neu Lym
e) BAL absolute cell composition
Cell count. 10³
f)
Masson's trichrome
CS + poly-(I:C)
CXCR4 lox/lox
CXCR4 lox/lox / Cre2ERT2
50 µm
g)
Standardized fibrosis (%)
h)
End-systole
End-diastole
2 mm
i) Wall thickness
Wall thickness (mm)
LV Septum RV
j) Fulton
Fulton index
k) RVSP
RVSP (mmHg)

Figure 5

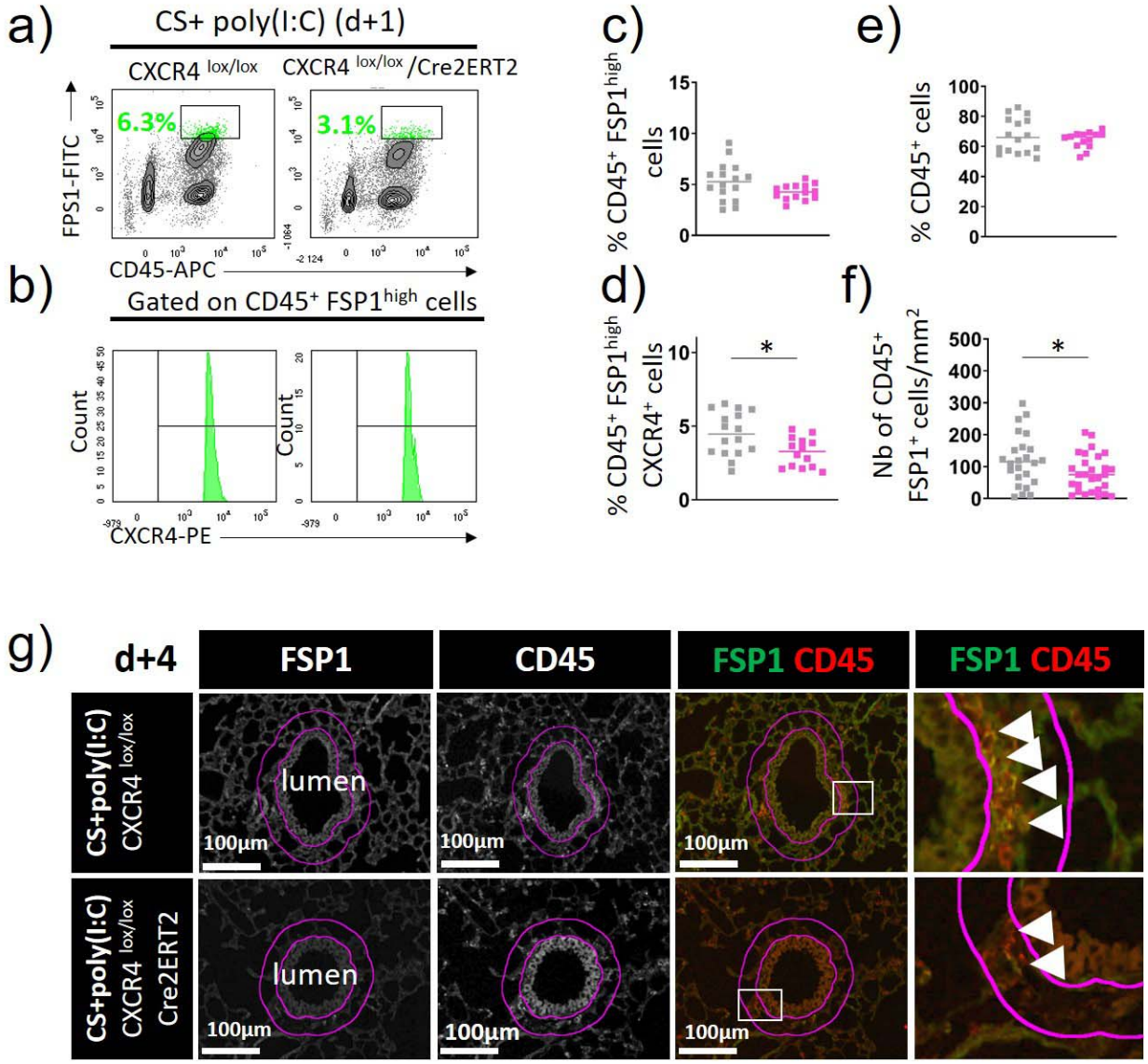
a)
CS+ poly(I:C) (d+1)
CXCR4 lox/lox
CXCR4 lox/lox /Cre2ERT2
6.3%
3.1%
FPS1-FITC
CD45-APC
b)
Gated on CD45+ FSP1high cells
Count
CXCR4-PE
c)
% CD45+ FSP1high cells
d)
% CD45+ FSP1high CXCR4+ cells
e)
% CD45+ cells
f)
Nb of CD45+ FSP1+ cells/mm2
g)
d+4
FSP1
CD45
FSP1 CD45
FSP1 CD45
CS+poly(I:C) CXCR4 lox/lox
CS+poly(I:C) CXCR4 lox/lox Cre2ERT2
lumen
100µm

Figure 6

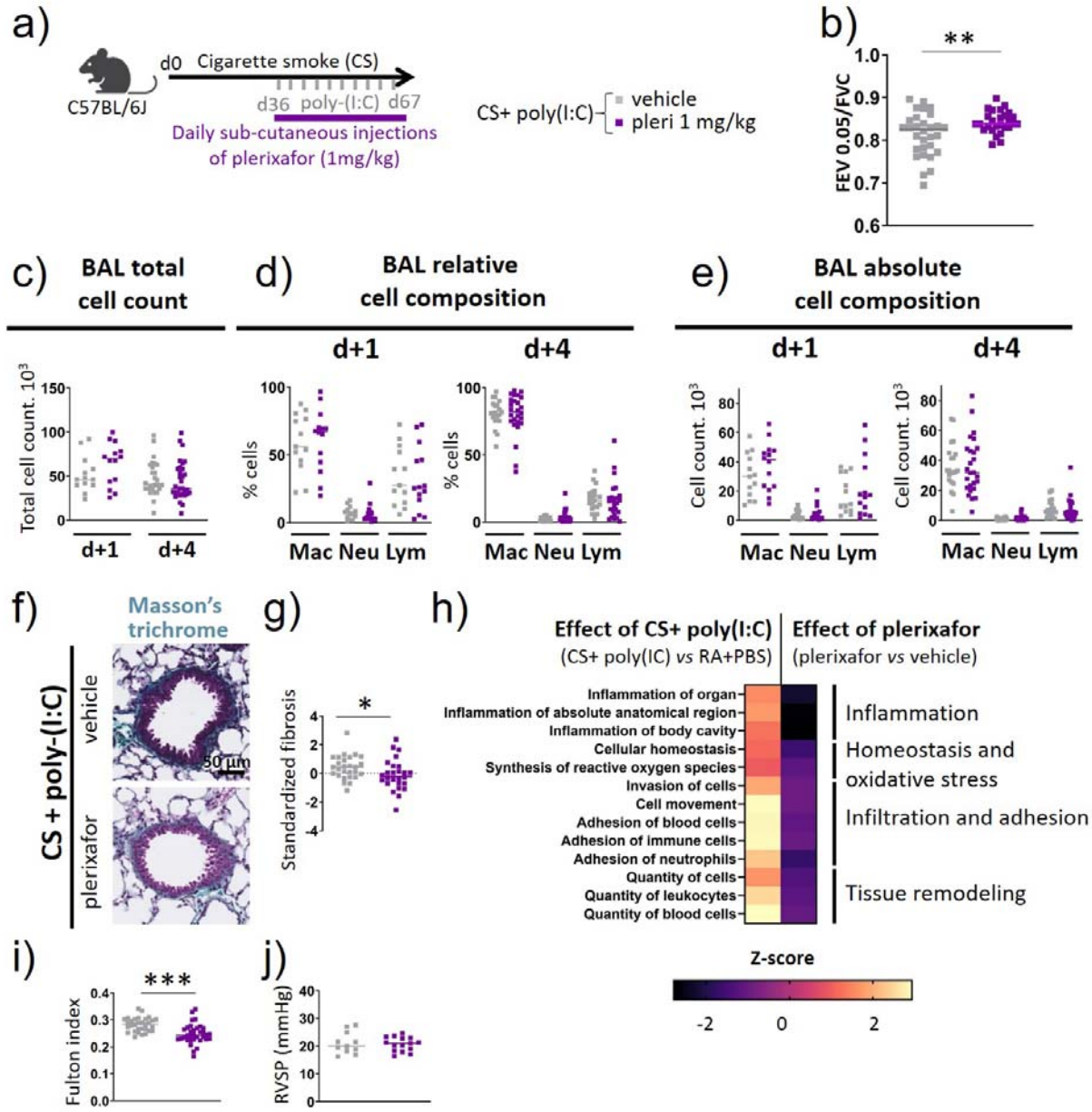
a)
C57BL/6J
d0 Cigarette smoke (CS)
d36 poly-(I:C) d67
Daily sub-cutaneous injections of plerixafor (1mg/kg)
CS+ poly(I:C)
vehicle
pleri 1 mg/kg
b)
FEV 0.05/FVC
**
c) BAL total cell count
Total cell count. 10³
d+1
d+4
d) BAL relative cell composition
% cells
Mac Neu Lym
e) BAL absolute cell composition
Cell count. 10³
f)
Masson's trichrome
CS + poly-(I:C)
vehicle
plerixafor
50 µm
g)
Standardized fibrosis
*
h)
Effect of CS+ poly(I:C)
(CS+ poly(IC) vs RA+PBS)
Effect of plerixafor
(plerixafor vs vehicle)
Inflammation of organ
Inflammation of absolute anatomical region
Inflammation of body cavity
Cellular homeostasis
Synthesis of reactive oxygen species
Invasion of cells
Cell movement
Adhesion of blood cells
Adhesion of immune cells
Adhesion of neutrophils
Quantity of cells
Quantity of leukocytes
Quantity of blood cells
Inflammation
Homeostasis and oxidative stress
Infiltration and adhesion
Tissue remodeling
Z-score
i)
Fulton index
***
j)
RVSP (mmHg)